Role of Vertical Mixing Originating From Small Vertical Scale Structures above and within the Equatorial Thermocline in an OGCM

Wataru Sasaki[1], Kelvin J. Richards[2], Jing-Jia Luo[3], Sebastien Masson[4], Swadhin K. Behera[3], Yukio Masumoto[3], and Toshio Yamagata[1,5]

[1]Application Laboratory, Japan Agency for Marine-Earth Science and Technology, Yokohama, Japan

[2]International Pacific Research Center/SOEST, University of Hawaii at Manoa, Honolulu, Hawaii, USA

[3] Research Institute for Global Change, Japan Agency for Marine-Earth Science and Technology, Yokohama, Japan

[4]Laboratoire d'Océanographie Expérimentation et Approches Numériques, CNRS, UPMC, IRD, Paris, France

[5]Department of Earth and Planetary Physics, Graduate School of Science, University of Tokyo, Tokyo, Japan

Corresponding author address: Wataru Sasaki, Application Laboratory, Japan Agency for Marine-Earth Science and Technology, 3173-25 Showa-machi Kanazawa-ku Yokohama Kanagawa Japan.
E-mail: wsasaki@jamstec.go.jp

Abstract

Recent high vertical resolution measurements show small vertical scale structures (SVSs) of the shear of ocean current are present above and within the equatorial thermocline. We investigate the impact of the mixing induced by the SVSs on the state of the equatorial Pacific in an ocean general circulation model (OGCM). The SVSs are typically unresolved in OGCMs and thus their impact needs to be parameterized. As a first step to determine the importance of the SVS induced mixing we introduce an enhanced mixing within and above the equatorial thermocline. It is found that this enhanced mixing reduces the stratification above the thermocline, and sharpens the thermocline through the Phillips effect [*Phillips*, 1973]. The sharpened thermocline limits the exchange of heat across the thermocline and traps the surface heating above the thermocline. The reduced stratification leads to less cooling of the mixed layer through entrainment, a reduced annual cycle and an increase in the annual mean of the sea surface temperature (SST) in the eastern equatorial cold tongue. The depth dependency in enhanced SVS mixing is crucial to its impact. When the enhanced mixing is applied throughout the depth of the ocean the cold tongue SST is cooled further. In the western equatorial Pacific, where the thermocline is deeper, SVS enhanced mixing induces a colder SST. We also find that the SVS mixing reduces the eddy kinetic energy associated with the tropical instability waves through a reduction of the meridional and vertical shear of the equatorial currents and temperature gradient.

1. Introduction

Vertical mixing of water properties and momentum are key processes that control the state of the tropical ocean. For this reason, numerous ocean modeling studies have focused on the development and refinement of the parameterization of vertical mixing in ocean general circulation models (OGCMs) [e.g. *Pacanowski and Philander* 1981; *Blanke and Delecluse* 1993; *Large et al.* 1994; *Noh et al.* 2005; *Zaron and Moum* 2009]. In these cases the focus has been on the vertical mixing induced by resolved processes in the OGCMs. Meanwhile unresolved vertical processes are tucked away as a "background" vertical diffusivity.

Previous studies have suggested that the background vertical diffusivity influences the coupled atmosphere-ocean system in the eastern equatorial Pacific [*Meehl et al.* 2001; *Richards et al.* 2009; *Fedorov et al.* 2010]. *Meehl et al.* [2001] found that a reduction in vertical diffusivity causes an increase in the amplitude of ENSO variability in a coupled general circulation model (CGCM). *Richards et al.* [2009], from a regional atmosphere-ocean coupled model simulation, found that a decrease in the background vertical mixing decreases the zonal asymmetry (a warmer cold tongue SST and decreased easterly winds) and increases the meridional asymmetry (an increased north-south temperature difference and increased southerlies). Mixing away from the equator also affects the system. *Fedorov et al.* [2010] found that increased extra-tropical vertical mixing leads to a warming of the cold tongue SST in a CGCM. These studies strongly suggest that the tropical climate system is sensitive to the vertical mixing associated with unresolved processes.

Recent measurements of ocean currents available at high vertical resolution capture vertical scales down to the order of O(2m). These new measurements showed numerous small vertical scale structures (SVSs) are present in and above the thermocline in the western equatorial Pacific [*Richards et al.*, 2011]. The SVSs are found to dominate the shear giving a peak in shear spectrum at vertical scales (inverse vertical wavenumber) between 5-10m. A peak in the shear spectrum at similar scales was also found by *Gregg et al.* [1996] and *Peters et al.* [1991] in the western and eastern tropical Pacific, respectively. *Richards et al.* [2011] found that active mixing (as determined by the turbulent kinetic energy dissipation rate) is strongly related to the SVSs and there are large differences between El Niño and La Niña conditions. In the latter case the estimated vertical diffusion coefficient was found to vary from 10^{-5} to 10^{-3} m^2s^{-1} from the core of the thermocline to the base of the surface mixed layer. This is in stark contrast to the estimated diffusion coefficients below the thermocline in equatorial waters, which is found to be as low as 10^{-6} m^2s^{-1} [*Gregg et. al*, 2003]. The physical processes responsible for the presence of the SVSs are still under investigation, but are likely to be instabilities of the larger scale currents (inertial and parametric instabilities: *Natarov and Richards*, 2009) and wind generated high vertical mode near inertial waves.

The vertical scale of the SVSs is such that they are unresolved in OGCMs with conventional vertical resolution. The observations strongly suggest that OGCMs are missing important physics with regard to ocean vertical mixing in and above the equatorial thermocline. The vertical mixing originating from the SVSs, therefore, needs to be parameterized and its impact investigated. In this study, as a first step towards gaining an understanding of the likely role of SVS induced mixing in the dynamics of the equatorial ocean we employ a simple method for parameterization of the SVS mixing, and focus on the impacts of the SVS mixing on the climatological state of the equatorial Pacific.

The rest of this paper is structured as follows: the OGCM is introduced in section 2 and we describe the experimental design, Section 3 presents the effects of SVS mixing on the equatorial Pacific, and Section 4 provides summary and discussions.

2. Model Description and Experimental Design

2.1. OGCM

The OGCM used in this study is the NEMO modeling system [*Madec*, 2006], which includes the ocean model Océan Parallélisé (OPA9). We employ the ORCA-R05 grid, which has a global configuration grid at 0.5° cos(lat) resolution. The OPA9 with the ORCA-R05 grid has 31 vertical levels with the first 14 levels lying in the top 150 meters. Oceanic vertical eddy diffusivity and viscosity coefficients are calculated from a 1.5-order turbulent closure scheme [*Blanke and Delecluse*, 1993]. In the turbulent closure scheme, the background vertical diffusivity coefficient is defined as the lower limit of the vertical diffusion coefficient. We retain this technique of specifying the background diffusivity in the experiments reported here, but note that specifying the background diffusivity by "adding" a value to the calculated value of the diffusion coefficient does not unduly affect the results (in the case of SST, the impact of changing the way the background diffusivity is specified is found to be an order of magnitude smaller than that of changing the value of the diffusivity itself).

The atmospheric forcing for the OGCM experiments is taken from the CORE (Coordinated Ocean-ice Reference Experiments) normal year forcing based on the

NCEP/NCAR reanalysis [*Large and Yeager*, 2004]. We utilize the following variables; 6-hourly varying 10m air temperature, specific humidity, and zonal and meridional marine wind vectors, daily varying surface downward shortwave and longwave radiation, and monthly varying rain and snow. The latent and sensible heat fluxes are calculated from the bulk formula according to the *Large and Yeager* [2004].

The model is initialized by setting the temperature and salinity equal to *Levitus* [1982], and a state of the rest. We have integrated the OGCM for 15 years, and analyzed the climatological annual mean for the last 5 years using output of 5-day means (we find that the ten year spin-up is sufficient for the tropical ocean to reach an equilibrium). Two experiments were integrated for a further 5 years (CTL and DEP20_LEV05, see below) and daily-mean output generated to allow an investigation of the impact of the SVS mixing on the eddy heat advection associated with tropical instability waves (TIWs), described in section 3.3.

2.2. Parameterization of SVS Mixing and Experimental Design

We have performed simulations with and without parameterized SVS mixing. Only the background vertical diffusivity coefficients are different between the simulations.

For the control run (CTL: without SVS mixing), the background vertical diffusivity coefficient is set to be a constant 1.0×10^{-6} m^2s^{-1} throughout the water column in the whole computational domain. The low value for the background vertical diffusivity coefficient is chosen because of the observation of low values at low latitudes [*Gregg et al.*, 2003].

In the runs with SVS mixing, the background vertical diffusivity coefficient in the equatorial Pacific is elevated to represent enhanced vertical mixing associated with SVSs, which are unresolved by the OGCM. The spatial pattern and temporal variation of the magnitude of the SVS mixing are unclear due to lack of sufficient high-resolution measurements. As the first step to include the effect of the SVS mixing and to understand the fundamental role of the SVS mixing, we propose a simple parameterization. Although likely to be important, here we exclude the temporal dependency of the magnitude of SVS mixing. Instead, we investigate the sensitivity of the solution to the magnitude and the vertical distribution of the SVS mixing. To reflect the observation that SVS enhanced mixing appears to occur in the upper water column down to the center of the thermocline [*Richards et al.*, 2011] the background diffusivity in the model is enhanced above a specified isotherm (DEP). The center of the model thermocline is at approximately DEP=20°C across the width of the Pacific basin. We choose two other depths, DEP=15°C and 0°C, to investigate the sensitivity to the specified depth (in the latter case mixing is enhanced throughout the water column). The level of SVS enhanced mixing is set by LEV. We vary LEV from 0 (CTL) to 1×10^{-4} m^2s^{-1}. Below DEP the background diffusivity is set to the control value of 1.0×10^{-6} m^2s^{-1} (we specify a smooth transition between the two values of diffusivity over a relatively small depth interval). The full range of experiments is provided in Table 1. Two examples of the variation of background diffusivity at the model grid points on the equator and 160°E are shown in Fig. 1. The enhanced diffusivity is applied to the tropical Pacific (5°S-5°N, 140°E-70°W). To investigate the sensitivity to the vertical distribution of the SVS enhanced mixing we perform an additional experiment where the background diffusivity is increased linearly from DEP=15°C to a value of 1×10^{-4} m^{2}s^{-1} at the base of the mixed layer (see LEVvar in Table 1). We note that our experiments differ from those of *Meehl et al.* [2001] and *Richards et al.* [2009] who consider a constant background vertical diffusivity. In our case the background diffusivity is allowed to vary with depth. As we will see, this variation with depth has a large impact on the model solution.

3. Results

We briefly evaluate the OGCM performance in terms of the capturing the observed annual mean and annual cycle of SST, and annual mean of zonal currents in the tropical Pacific.

Fig. 2a shows the annual mean SST for the tropical Pacific in the CTL. The warm pool SST (WPSST) and the cold tongue SST (CTSST) are well simulated. However, the CTSST in the run without SVS mixing (CTL) is up to approximately 1°C too cold (red line in Fig. 3a). On the other hand, the WPSST in the run without SVS mixing is positively biased by about 0.5°C (red line in Fig. 3a). These positive and negative SST biases lead to a steeper zonal gradient of SST along the equatorial Pacific. Comparing the amplitude of the annual cycle in CTL at 0°N, 120°W with observations we find that the modeled SST annual cycle is greater than that of observed (red and black dotted lines in Fig. 3b). The modeled SST in Fig. 3b contains the intra-monthly variability since the output interval of the model is kept at 5-day. On the other hand the observed SST lacks the intra-seasonal variability since the dataset is monthly averaged. Even allowing for the strong intra-seasonal variability in the modeled SST, the modeled SST in the eastern equatorial Pacific is negatively biased particularly during July-February (Fig. 3b). The observed small amplitude of the annual cycle of SST in the western equatorial Pacific is well simulated (Fig. 3b), even though the modeled SST is positively biased throughout the year.

The 20°C isotherm depth, representing the thermocline depth, and the 16°C and 22°C isotherms, whose depth difference is used as a measure of the thickness of the thermocline, are shown in Fig. 2b for CTL and observation. The thermocline depth shoaling toward the east in the equatorial Pacific is reasonably well simulated as observed. The thermocline depth in the CTL is shallower than that observed. On the other hand, the thermocline thickness in the eastern equatorial Pacific in the CTL is comparable to that observed. The shallower thermocline is consistent with the stronger annual cycle of SST in the eastern equatorial Pacific, since it is easier for equatorial upwelling to tap the colder sub-thermocline water with shallower thermocline for a given wind variation [*Meehl et al.*, 2001] (as seen in Fig. 3b).

Figs. 2d and e compare the annual mean of zonal current along the equatorial Pacific between observation and CTL. The jet-like structure of the equatorial undercurrent (EUC) is well simulated as observed, although the magnitude of the modeled EUC is up to 0.2 ms^{-1} stronger than that of observed. In association with the too-strong EUC, the modeled westward surface current is weaker than that of observed (Figs. 2d and e). The too-strong EUC in the CTL might be due to lack of lateral diffusivity originating from the interleaving process in the OGCM [*Pezzi and Richards*, 2003].

In summary, SST in the equatorial Pacific is qualitatively well simulated by the CTL of our OGCM, although the modeled SST in the equatorial Pacific is biased to some extent compared to the observed SST in terms of the annual mean and the amplitude of the annual cycle. The EUC is also well simulated by CTL of our OGCM in terms of the structure, although the magnitude of the modeled EUC is too strong compared to that observed. In the next section, impacts of SVS mixing on SST in the equatorial Pacific are described.

3.1 Impact of SVS mixing on the annual mean

Fig. 4 shows differences in the annual mean of SST simulated by the OGCM with and without SVS mixing. SSTs in the equatorial Pacific, Costa Rica Dome [*Wyrtki*, 1964], and the coastal region of Peru are strongly affected by the SVS mixing. The annual mean of the CTSST simulated by the OGCM with SVS mixing, except DEP0_LEV05, is warmer than that without SVS mixing, while the WPSST simulated by the OGCM with SVS mixing is colder than that without SVS mixing. SSTs in the Costa Rica Dome and the coastal region of Peru have also become warmer by the SVS mixing.

The CTSST in DEP20_LEV05 is warmer than that in CTL by up to 1 °C (Fig. 4a). On the other hand, the CTSST in DEP0_LEV05 run is colder than that in CTL (Fig. 4c). The DEP15_LEV05 (i.e. when SVS mixing is applied down to the 15 °C isotherm) is approximately at the transition point between the CTSST being warmed and being cooled by the SVS mixing (Fig. 4b). We find, therefore, that the warming of the CTSST in simulations with SVS mixing is reduced as the depth to which SVS mixing is applied is deepened. A SST warming in the Costa Rica Dome and the coastal region of Peru is not excessively affected by changing the depth to be which SVS mixing is applied (Figs. 4a, b, and c).

The cooling of the CTSST found in the DEP0_LEV05 (Fig. 4c) is a typical response to elevated background vertical diffusivity throughout the water column. More specifically, the elevated background vertical mixing throughout the water column brings up the cold, deeper waters and reduces the temperature in the upper ocean. Such a cooling of the CTSST by elevated background vertical diffusivity throughout the water column is also simulated in a regional atmosphere-ocean coupled model [*Richards et al.*, 2009].

The marked difference in the SST response between DEP20_LEV05 and DEP0_LEV05 when SVS mixing is introduced highlights the importance of the vertical distribution of the enhanced mixing.

For a fixed vertical distribution (DEP=20°C) the warming in the CTSST and a cooling of the WPSST are enhanced as the magnitude of the SVS mixing is elevated (Figs. 4a, d, and e). The warming of SST in the Costa Rica Dome and the coastal region of Peru is also enhanced as the magnitude of the SVS mixing is elevated (Figs. 4a, d, and e).

There is also a marked difference in the annual mean of SST between DEP15_LEV05 and DEP15_LEVvar (Figs. 4b and f), even though the isotherm-depth mean of the background vertical diffusivity coefficient for both runs are nearly equal to each other. A cooling of the WPSST is dominant in DEP15_LEV05 (Fig. 4b), while a warming of the CTSST is significant in DEP15_LEVvar (Fig. 4g). We discuss the cause of the difference in SST between the two runs in section 3.3.

The changes to the subsurface temperature and zonal component of velocity along the equator induced by SVS mixing are shown in Fig. 5 (the CTL is shown in Fig. 2). Quantitative measures of the depth of the 20°C isotherm and thermocline thickness at 3 longitudes are given in Table 2 for all experiments. There are marked differences in the changes depending on the depth where the enhanced mixing is specified. With a depth independent enhancement (DEP0_LEV05) there is a general broadening of the thermocline and associated cooling/warming above/below the 20°C isotherm. When the SVS mixing is restricted to above the 20°C, the thermocline sharpens and there is a general warming of the thermocline. The reasons for the sharpening of the thermocline are discussed in section 3.3. In the eastern half there is a warming throughout the water column above the thermocline.

Table 3 provides quantitative measures of the position of the core of the EUC at 3 longitudes for all experiments. There is a general deepening of the core of the EUC. For a fixed vertical distribution (DEP=20°C) the core of the EUC in the eastern equatorial Pacific is deepened as the magnitude of the SVS mixing is elevated. With a depth independent enhancement (DEP0_LEV05), there is a broadening of the EUC and associated strengthening/weakening in the lower/upper part of the EUC (Fig. 5f), which is a typical response to the elevated vertical mixing throughout the water column. Restricting the SVS mixing depth to be above the 20°C isotherm, there is a deepening of the EUC (Table 3) and associated strengthening in the lower part of the EUC (Fig. 5d).

3.2 Changes in the Annual Cycle of SST

Does a warming of the annual mean of the CTSST (Fig. 4) in simulations with SVS mixing take place throughout the year? To answer this question, we investigate changes in the annual cycle of SST along the equatorial Pacific. Fig. 2c shows the annual cycle of SST along the equatorial Pacific simulated in CTL. A warming of the CTSST during boreal spring associated with both the passage of solar zenith and reduced cloud cover during the period [*Kessler et al.*, 1998] is well simulated by the ocean model. Fig. 6a shows a difference in the annual cycle of SST along the equatorial Pacific between DEP20_LEV05 and CTL. A warming of the CTSST exceeds 1°C during July-February, while a warming of the CTSST during March-June is much less. This result reveals that the warming of the annual mean of the CTSST in DEP20_LEV05 (Fig. 4a) is due to a SST warming during the second half of the year (July-February). A warming of the CTSST during the second half of the year is also found in other simulations with SVS mixing (Fig. 6).

On the other hand, the CTSST during boreal spring-summer in DEP15_LEV05 and DEP0_LEV05 is colder than that in CTL (Figs. 6b and c). This result reveals that the colder annual mean of SST in DEP15_LEV05 and DEP0_LEV05 (Figs. 4b and c) is due to the cooling during boreal spring-summer (Figs. 6b and c).

Hereafter, we mainly focus on the DEP20_LEV05, DEP20_LEV1, and DEP0_LEV05 to compare the impact of the magnitude of SVS mixing and the depth to which it is applied.

3.3. Changes in Mixed Layer Heat Budget in the Cold Tongue

To understand the mechanism of changes in the CTSST caused by SVS mixing, we examine the heat budget of the mixed layer (ML) in the eastern equatorial Pacific (2°S-2°N, 160°W-80°W). The ML temperature (*T_m;* MLT) evolution is given by the following equation [e.g. *Menkes et al.*, 2006].

$$\begin{aligned}\frac{\partial T_m}{\partial t} &= \underbrace{-\left< u\frac{\partial T}{\partial x} + v\frac{\partial T}{\partial y} + w\frac{\partial T}{\partial z} \right>}_{A} + \underbrace{\left< D_l(T) \right>}_{B} \\ &\underbrace{-\frac{1}{h}\frac{\partial h}{\partial t}[T - T(z=h)] + \frac{1}{h}\left(K_z\frac{\partial T}{\partial z}\right)(z=h)}_{C} + \underbrace{\frac{Q_* - Q_s[1 - f(z=h)]}{\rho_0 C_p h}}_{D}\end{aligned} \tag{1}$$

where the angle brackets denote a vertical average over the depth of the ML, *h*. The ML depth (MLD) is calculated as the depth where the density is 0.05 kg m^{-3} higher than the surface density as used in *Menkes et al.* [2006] and *Cravatte and Menkes* [2009]. In Eq. (1), term A (advection term) represents the advection of temperature by horizontal and vertical currents, term B represents the lateral diffusion, and term C (vertical diffusion term) represents the exchanges between the ML and the deeper ocean. The last term includes the diffusive flux term and entrainment through the ML base. The term D (atmospheric forcing term) represents the net surface heat flux absorbed by the ML. In our experiments, the entrainment is calculated as the residual between the left-hand side in Eq. (1) and terms A, B, D, and the diffusive flux term.

Fig. 7a shows the annual cycle of the term A, B, C and D for the ML in the cold tongue in CTL. A warming by the surface heat fluxes and a cooling by the vertical diffusion are balanced as shown in earlier studies [*Menkes et al.*, 2006; *Cravatte and Menkes*, 2009]. The lateral diffusion term is negligible throughout the year. Temperature tendency shows significant intra-monthly variability particularly during boreal fall. The intra-monthly variability of the temperature tendency coincides well with that of the advection term. The intra-monthly variation of the advection term is related to the TIW activity [*Cravatte and Menkes*, 2009]. The impact of SVS mixing on the TIW activity is discussed in section 3.5.

In the experiments with depth dependent SVS mixing (DEP20_LEV05 and DEP20_LEV1) there is a reduced warming by the atmospheric fluxes and a reduced cooling by vertical diffusion (Figs. 7b and d). The reduced atmospheric forcing is due to a warmer MLT which induces greater loss of latent heat, longwave radiation, and sensible heat. Therefore the reduction of the atmospheric forcing is the result rather than the cause of the SST warming. These results indicate that the warming of the CTSST in simulations with SVS mixing is induced by a reduction in diffusion in the second half of the year. For instance, the vertical diffusion term in DEP20_LEV1 is around $-0.1\,^{\circ}$C/day during August-November (Fig. 7d), while that in CTL is less than $-0.2\,^{\circ}$C/day (Fig. 7a). A weakening of the cooling by vertical diffusion during August-November is also seen in DEP20_LEV05 (Fig. 7b).

Fig. 8 shows the atmospheric forcing, advection, and vertical diffusion terms for the ML of the cold tongue averaged for the second half of the year. The warming by atmospheric fluxes is balanced with a cooling by vertical diffusion in the time averaging (right and left parts of Fig. 8). On the other hand, the advection term averaged for the second half of the year is negligible (central part of Fig. 8). There is a notable reduction in the cooling by vertical diffusion when depth dependent SVS mixing is applied, with the reduction increasing with the level of enhanced mixing. This clearly indicates that the warmer MLT during the second half of the year in the DEP20 runs is caused by a reduction of vertical diffusion. This is in stark contrast to the colder cold tongue and increased cooling by vertical diffusion when the enhanced mixing is applied throughout the depth of the water column (green bar in Fig. 8).

Fig. 9 shows the atmospheric forcing, advection, and vertical diffusion terms for the ML of the CT averaged for the first half of the year (March-June). Now advection plays a somewhat larger role (although it is still small). The changes induced by depth dependent SVS mixing are much less than those in the second half of the year, while those induced by depth independent enhanced mixing are somewhat greater.

In summary, a warmer CTSST during the second half of the year in simulations with depth dependent SVS mixing is caused by a weaker cooling associated with weakened vertical diffusion.

The vertical diffusion term consists of the entrainment and diffusive flux terms. The entrainment term is negligible compared to the diffusive flux term in our experiments (Figure not shown). The diffusive flux, $\frac{1}{h}(K_z \frac{\partial T}{\partial z})_{z=h}$, depends on the MLD ($h$), vertical diffusivity coefficient (K_z), and vertical gradient of temperature ($\frac{\partial T}{\partial z}$) at the ML base. From the formulation of the diffusive flux, it is obvious that a thicker ML, weaker vertical gradient of temperature, and weaker vertical mixing contribute less to cool the MLT. Fig. 10a shows the annual cycle of the stratification (in terms of the square of the buoyancy frequency), mixed layer depth and depth of the 20°C isotherm averaged between 2°S- 2°N, 120°W-100°W for the CTL. A particular feature to note is the shoaling of the thermocline in the second half of the year. Figs. 10b and d show the changes in the stratification and vertical diffusivity when depth limited SVS mixing is introduced. The enhanced mixing above the thermocline produces a sharpening of the thermocline and a much-reduced stratification (and vertical temperature gradient) above the thermocline. The reduced stratification leads to an increase in the vertical diffusivity which feeds back to further reduce the stratification and tighten the thermocline (the so-called "Phillips effect"; *Phillips*, 1972). The reduced stratification (and warmer temperature, recall Fig. 5) allows the deepening of the mixed layer in the second half of the year, and produces a reduced cooling of the mixed layer because of the reduced temperature gradient and warmer temperature (Fig. 5a), despite the increase in vertical diffusivity.

The increase in vertical diffusivity associated with the reduction of the stratification leads to a reduction of the magnitude of the upper part of the EUC (Fig. 5d). The reduction of the magnitude of the upper EUC reduces the vertical shear of the current, which in turn reduces the vertical diffusivity in the layer. This reduction of the upper EUC, therefore, works to weaken the Phillips effect to some extent. In contrast, a depth independent increase in the background mixing (DEP0_LEV05; Fig. 10c) weakens the thermocline and brings cooler water to the base of the mixed layer (Fig. 5c). This has the effect of slightly reducing the depth of the mixed layer and increasing the cooling of the mixed layer through vertical diffusion (again, despite the decrease in vertical diffusivity).

Fig. 11 shows the background vertical diffusivity coefficients for the DEP20_LEV05, DEP15_LEV05 and DEP15_LEVvar. The background vertical diffusivity for the DEP15_LEVvar is much closer to that of the DEP20_LEV05 (changes in SST in DEP15_LEVvar are also closer to those in DEP20_LEV05 than to DEP15_LEV05, recall Fig. 4). In case of DEP15_LEVvar, a relatively strong SVS mixing above the thermocline induces the Phillips effect to deepen and sharpen the thermocline and to increase the CTSST, while relatively weak SVS mixing below the thermocline does not bring up the cold water to diffuse the thermocline.

3.4. Changes in Mixed Layer Heat Budget in the Warm Pool

Fig. 12 shows the annual cycle of the tendency terms for the ML heat budget in the western equatorial Pacific in the CTL and SVS runs. The annual mean of the various terms is shown in Fig. 13. The atmospheric forcing and vertical diffusion terms show two peaks during boreal spring and autumn (Fig. 12), which are due to the passage of the solar zenith. Advection contributes to cool the mixed layer. Introducing SVS enhanced mixing leads to an increase in the cooling due to vertical diffusion and advection. Note that the cooling occurs for both the depth dependent and independent cases.

Fig. 14 shows the annual cycle of stratification, mixed layer depth, depth of the 20°C isotherm and vertical diffusivity in the western equatorial Pacific for the CTL. The thermocline depth in the WP is much deeper and the annual cycle is much weaker than that in the CT (Figs. 10 and 14). Fig. 14c shows the changes in the stratification and vertical diffusivity when depth independent SVS mixing (DEP0_LEV05) is introduced. The depth independent SVS mixing weakens the thermocline and brings cooler water to the base of the mixed layer. The mechanism of the cooling of WPSST is the same as that of a cooling of CTSST (section 3.3).

Figs. 14b and d show the changes in the stratification and vertical diffusivity when depth limited SVS mixing is introduced. The SVS enhanced mixing above the thermocline sharpens the thermocline and a much-reduced stratification above the thermocline. The vertical diffusivity above the mixed layer depth is much reduced, while stratification is not changed much. The difference in SST response to the depth limited SVS mixing between WP and CT may be due to the distance between the mixed layer and the thermocline. In fact the response of the CTSST is weak from March to June during which the thermocline is deep.

3.5. Impact of SVS mixing on Tropical Instability Waves

Although SVS mixing does not affect an advection term in the ML in the eastern equatorial Pacific during the second half of the year (central part of Fig. 8), it is interesting to understand impacts of SVS mixing on the eddy advection associated with TIW activity. To evaluate impacts of the SVS mixing on the eddy advection, an advection term is decomposed into the following four terms; the advection of mean temperature by mean current ($-\overline{U}\nabla\overline{T}$), the advection of eddy temperature by mean current ($-\overline{U}\nabla T'$), the advection of mean temperature by eddy current ($-U'\nabla\overline{T}$), and the advection of eddy temperature by eddy current ($-U'\nabla T'$), where $\overline{U}=(\overline{u},\overline{v},\overline{w})$ and $U'=(u',v',w')$ denote the mean and the eddy current field, respectively. $\overline{T}$ and T' represents the mean and eddy temperatures, respectively.

$$-(u\frac{\partial T}{\partial x}+v\frac{\partial T}{\partial y}+w\frac{\partial T}{\partial z})=-\overline{U}\nabla\overline{T}-\overline{U}\nabla T'-U'\nabla\overline{T}-U'\nabla T' \quad (2)$$

The mean field is obtained by applying a 70-day running-mean filter to daily mean field from a 5-yr simulation. The eddy field is obtained by subtracting the mean field from the daily mean field. The mean advection term $-\overline{U}\nabla\overline{T}$ therefore represents the advection of low-frequency temperature by low-frequency currents. The eddy advection term representing the effects of eddies is defined as $-\overline{U}\nabla T'-U'\nabla\overline{T}-U'\nabla T'$.

Fig. 15a shows the annual mean of the eddy kinetic energy (EKE) averaged from the surface to 100m depth. The EKE is defined as $\frac{1}{2}\rho_0(U'^2+V'^2)$, where ρ_0 is the density. The EKE of the CTL has a peak at 2°-4°N in the eastern equatorial Pacific, as simulated in *Small et al.* [2009]. The EKE of DEP20_LEV05 is weaker than that of the CTL (Fig. 15b).

Fig. 16 shows the monthly means of the mean and eddy advection terms in the eastern equatorial Pacific for CTL and DEP20_LEV05. The mean advection term is negative throughout the year, indicating that the mean advection tends to cool the MLT in the eastern equatorial Pacific. In contrast, the eddy advection warms the MLT in the eastern equatorial Pacific particularly during boreal summer and autumn (Fig. 14). These results are consistent with results based on observations [*Wang and McPhaden*, 1999; *Jochum et al.*, 2007] and OCGM experiments [*Cravatte and Menkes*, 2009; *Richards et al*, 2009]. The introduction of SVS mixing reduces the cooling due to the mean advection, particularly during the second half of the year, when compared to the CTL. This reduced cooling by the mean advection is compensated by a reduced warming by the eddy flux. As a result, SVS mixing reduces the amplitude of the annual cycle of both the mean and eddy advective heat fluxes, while producing virtually no change to the total advective heat flux (Figs. 8 and 9). The changes in mean and eddy fluxes are explained by changes in barotropic (BT) and baroclinic (BC) conversion rates defined, e.g. [*Small et al.*, 2009], by

$$BT = -\rho_0 \left\langle u' \bullet \left(u' \bullet \frac{\partial U}{\partial x}, u' \bullet \frac{\partial U}{\partial y} \right) \right\rangle$$
$$BC = -g \left\langle \rho' w' \right\rangle$$

where angle bracket denotes a depth average, u' and U are the depth dependent ocean eddy and large scale current, respectively. Fig. 15c shows the depth average and longitude average of the BT and BC for the CTL. The BT has a peak near the equator due to the meridional shear between the EUC and north branch of the South Equatorial Current, while the BC has a peak at around 3°N due both to temperature gradient and vertical shear of the equatorial currents [*Small et al.*, 2009]. The BT and BC are reduced in the DEP20_LEV05 (Fig. 15d). This result reveals that the EKE associated with the

TIW is weakened due both to the reduction of the meridional and vertical shear of the equatorial currents and temperature gradient.

4. Summary and Discussion

Small Vertical Scale structures (SVSs) have been observed to contribute greatly to vertical mixing in and above the equatorial thermocline. Their scale is such that they are typically unresolved by OGCMs. We have investigated the role of the elevated vertical mixing induced by the SVSs in the thermocline in the equatorial Pacific. It has been found that the elevated background vertical mixing affects the state of equatorial Pacific. We have found that the enhanced mixing sharpens the thermocline and reduces the stratification above the thermocline through the Phillips effect [*Phillips*, 1973]. The sharpened thermocline limits the exchange of heat across the thermocline and tends to trap heat above the thermocline in the eastern equatorial Pacific. The reduced stratification allows the mixed layer to deepen more during times of entrainment but leads to less cooling of the mixed layer and hence SST. The amplitude of the annual cycle in SST is reduced and the annual mean SST increased when compared to the case with no SVS enhanced mixing. These changes are in stark contrast to those obtained when the background vertical diffusivity coefficient is enhanced throughout the depth of the water column, which leads to a more diffuse thermocline, greater cooling during entrainment and a colder annual mean SST

SVS-induced mixing also reduces the stratification, and sharpens and deepens the thermocline in the western equatorial Pacific. The thermocline in the western equatorial Pacific, however, is much deeper than that in the eastern equatorial Pacific. The enhanced vertical mixing in the western equatorial Pacific brings up relatively cooler waters to reduce the temperature in the upper ocean.

It has been found that the mixing induced by SVSs reduces the amplitude of the annual cycle of both the mean and eddy advective heat fluxes, while producing virtually no change to the total advective heat flux. The mixing induced by SVSs reduces the EKE associated with the TIWs through a reduction of the meridional and vertical shear of the equatorial currents and temperature gradient.

Our work demonstrates the importance of the vertical distribution of the vertical mixing by unresolved processes (the background vertical diffusivity). We have chosen to use a particularly simple parameterization to show the role of mixing induced by SVSs. A more physically based parameterization scheme for the mixing induced by SVSs will need to take the generation mechanism into account. *Richards et al.* [2011] speculate that the observed SVSs are caused by a combination of instabilities of the flow and wind generated inertia-gravity waves. The SVS induced mixing will therefore be temporally and spatially variable. Indeed, *Richards et al.* [2011] find large differences in the vertical diffusivity in the western equatorial Pacific between El Niño and La Niña states, brought about principally by changes to the stratification between the bottom of the mixed layer and the main thermocline. This leads us to speculate on the possibility of feedbacks in the coupled system. A warmer cold tongue reduces the east-west pressure gradient in the atmosphere, which in turn reduces upwelling in the ocean further warming the cold tongue (the Bjerknes feedback, *Bjerknes* 1969; see also *Richards et al.* 2009). Initial experiments with a coupled model show the warming of the cold tongue when SVS mixing is added to be increased, as expected (results to be reported elsewhere). The vertical mixing induced by SVSs may thus reduce the strong cold SST bias in the eastern equatorial Pacific found in many CGCMs [*Lin*, 2007]. The link between SVS induced mixing and the ENSO state offers the possibility of further feedbacks that will be explored future studies.

Acknowledgments

This study was partially supported by the Japan Science and Technology Agency/ Japan International Cooperation Agency through Science and Technology Research Partnership for Sustainable Development (SATREPS) and the Grants-in-Aid for Scientific Research (C) from the Ministry of Education, Culture, Sports, Science and Technology of Japan. All experiments were performed on the Earth Simulator 2.

References

Bjerknes, J. (1969), Atmospheric teleconnections from the equatorial Pacific, *Mon. Wea. Rev.*, **97**, 163–172.

Blanke, B., and P. Delecluse (1993), Variability of the tropical Atlantic Ocean simulated by a general circulation model with two different mixed layer physics, *J. Phys. Oceanogr.*, **23**, 1363-1388.

Cravatte, S. and C. E. R. Menkes (2009), Sensitivity of mixed layer heat budgets to wind forcing: A case study for the equatorial Pacific cold tongue, *Ocean Modeling*, **29**, Issue 3, 198-212.

Fedorov, A. V., C. M. Brierley, and K. Emanuel (2010), Tropical cyclones and permanent El Nino in the early Pliocene epoch, *Nature*, **463**, 1066-1071.

Gregg, M. C., D. P. Winkel, T. B. Sanford, and H. Peters (1996), Turbulence produced by internal waves in the oceanic thermocline at mid and low latitudes, *Dyn. Atm. Oceans*, 24, 1-14.

Gregg, M. C., B. Sanford, and D. P. Winkel (2003), Reduced mixing from the breaking of internal waves in equatorial waters, *Nature*, **422**, 513-515.

Jochum, M., and R. Murtugudde (2005), Temperature advection by tropical instability wave, *J. Phys. Oceanogr.*, **36**, 592-605.

Kessler, W. S., L. M. Rothstein, and D. Chen (1998), The Annual Cycle of SST in the Eastern Tropical Pacific, Diagnosed in an Ocean GCM, *J. Clim.*, **11**, 777-799.

Large, W. G., J. C. McWilliams, and S. C. Doney (1994), Oceanic vertical mixing: A review and a model with a nonlocal boundary layer parameterization, *Rev. of Geophys.*, **32**, 4, 363-403.

Levitus, S. (1982), *Climatological Atlas of the World Ocean*, NOAA Prof. Paper 13, 173pp. and 17microfiche.

Lin, J.-L. (2007), The double-ITCZ problem in IPCC AR4 coupled CGMs: Ocean-Atmosphere feedback analysis, *J. Clim.*, 20, 4497-4525.

Madec, G. (2006), NEMO ocean engine, Note du Pole de Modelisation, Institut Pierre-Simon Laplace (IPSL).

McPhaden, M. J. (1985), Fine-structure variability observed in CTD measurements from the central equatorial Pacific, *J. Geophys. Res.*, **90**, C6, 11726-11740.

Meehl, G. A., P. R. Gent, J. M. Arblaster, B. L. Otto-Bliesner, E. C. Brandy and A. Craig (2001), Factors that affect the amplitude of El Nino in global coupled climate models, *Climate Dynamics*, **17**, 515-526.

Menkes, C. E. R., J. G. Vialard, S. C. Kennan, J.-P. Boulanger, G. V. Madec (2004), A Modeling study of the impact of tropical instability waves on the heat budget of the eastern equatorial Pacific, *J. Phys. Oceanogr.,*

Natarov and Richards (2009), Three-dimensional instabilities of oscillatory equatorial zonal shear flows, *J. Fluid Mech.*, **623**, pp.59-74.

Pacanowski, R., and S. G. H. Philander (1981), Parameterization of vertical mixing in numerical models of tropical oceans, *J. Phys. Oceanogr.*, **11**, 1443-1451.

Peters, H. M. C. Gregg, and T. B. Sanford (1991), Equatorial and off-equatorial fine-scale and large-scale shear variability at 140W, *J. Geophys. Res.*, **96**, C9, 16913-16928.

Pezzi, L. P., and K. J. Richards (2003), Effects of lateral mixing on the mean state and eddy activity of an equatorial ocean, *J. Geophys. Res.*, **108**, C12.

Phillips, O. M. (1972), Turbulence in a strongly stratified fluid - is it unstable?, *Deep Sea Res.*, **19**, 79-81.

Richards, K. J., S.-P. Xie, and T. Miyama (2009), Vertical mixing in the ocean and its impact on the coupled ocean-atmosphere system in the eastern tropical Pacific, *J. Clim*, **22**, 3703-3719.

Richards, K. J., Y. Kashino, A. Natarov, E. Firing (2011), Mixing in the western equatorial Pacific, and its modulation by ENSO, in preparation.

Small, R. J., K. J. Richards, S.-P. Xie, P. Dutrieux, and T. Miyama (2009), Damping of tropical instability waves caused by the action of surface currents on stress, *J. Geophys. Res.*, **114**, C04009.

Wrytki, K. (1964), Upwelling in the Costa Rica Dome, *Fish Bull.*, **63**, 2, 355-372.

Zaron, E. D., J. N. Moum (2009), A new look at Richardson number mixing schemes for equatorial ocean modeling, *J. Phys. Oceanogr.*, **39**, 2652-2664.

Table captions

Table 1. List of experiments. “DEP” denotes the isotherm to be which SVS mixing is applied (˚C). “LEV” denotes the magnitude of the SVS mixing (m^2s^{-1}). Details are described in the right column. Background vertical diffusivity coefficients associated with SVS mixing are computed at every time step. The background vertical diffusivity coefficients in the equatorial Pacific and those outside of the region are linearly interpolated (c.f. Fig. 1).

Table 2. The 20˚C isotherm depth (D_{20}) and thickness of thermocline (ΔD_{16-22}). The thickness of the thermocline is defined as the distance between isotherms of 16˚C and 22˚C. Unit is meter.

Table 3. Position of the core of the EUC, designated as the vertical grid point in which the annual mean of the zonal velocity averaged between 1˚S-1˚N has the maximum. Bold shows that the position of the core of the EUC of the run is deeper than that of CTL. Unit is meter.

Figure captions

FIG. 1 Background vertical diffusivity coefficients at 0˚N, 160˚E for (a) DEP20_LEV05 and (b) DEP15_LEV05. Unit is m^2s^{-1}.

Fig. 2 (a) The annual mean of SST in CTL. (b) The annual mean of temperature averaged over the latitudinal band 2˚S-2˚N simulated by the OGCM (black) and observed (red). The 16, 20, and 22˚C isotherms are shown for the observed temperature. (c) The annual cycle of SST averaged over the latitudinal band 2˚S-2˚N. (d) Observed annual mean of zonal current averaged over the latitudinal band 1˚S-1˚N. (e) As in (d), but for the zonal current simulated in CTL. Unit is ˚C for (a-d) and ms^{-1} for (d and e).

FIG.3 (a) The annual mean of SST averaged over the latitudinal band 2˚S-2˚N. (b) The annual cycle of SST at 0˚N, 170˚E (solid) and 0˚N, 120˚W (dotted). Black and red shows the observation and model result, respectively. Unit is ˚C.

FIG. 4 A difference in the annual mean of SST between simulations with and without SVS mixing (with minus without SVS mixing). Unit is ˚C. The contour interval is 0.5˚C.

Fig. 5 (a-c) A difference in the annual mean of temperature along the equator between simulations with and without SVS mixing (with minus without SVS mixing). The contour shows the isotherm line of 16, 20, and 22˚C. Unit is ˚C. (d-f) The annual mean of zonal current along the equator (contour) and a difference in the annual mean of the zonal current between simulations with and without SVS mixing (color). Unit is ms^{-1}

Fig. 6 As in Fig. 4, but for the annual cycle of SST averaged over the latitudinal band 2°S-2°N. The unit is °C.

Fig. 7 The annual cycle of the tendency terms for the mixed layer heat budget averaged over the region 2°S-2°N, 140°W-90°W in (a) CTL, (b) DEP20_LEV05, (c) DEP0_LEV05, and (d) DEP20_LEV1. Red shows the atmospheric forcing term. Blue shows the sum of the entrainment and diffusive flux at the mixed layer base. Cyan and purple denote the lateral diffusion and advection, respectively. Black shows the temperature tendency. The unit is °C day^{-1}.

Fig. 8 The tendency terms for the mixed layer heat budget averaged over the region 2°S-2°N, 140°W-90°W for the July-February mean in CTL (white), DEP0_LEV05 (green), DEP20_LEV05 (red), and DEP20_LEV1 (blue). The left, central, and right part show the atmospheric forcing, advection, and vertical diffusion term, respectively. Unit is °C day^{-1}.

Fig. 9 As in Fig. 7, but for the March-June mean.

Fig. 10 (a) The annual cycle of the square of the buoyancy frequency ($\times10^{-4}$ s^{-2}, contour) averaged over the region 2°S-2°N, 120°W-100°W in CTL. (b-d) Difference in the vertical diffusivity coefficient ($\times10^{-4}$ m^{2}s^{-1}, color shaded) and the square of the buoyancy frequency ($\times10^{-4}$ s^{-2}, contour) between simulations with and without SVS mixing, respectively. Contours in cyan and green denote the annual cycle of the mixed layer depth and 20˚C isotherm, respectively.

Fig. 11 (a) Vertical distribution of the annual mean of background vertical diffusivity coefficient averaged over the region 2˚S-2˚N, 120˚W-100˚W for DEP20_LEV05 (black), DEP15_LEV05 (red), and DEP15_LEVvar (green). The decimal logarithm is taken for the background vertical diffusivity coefficient. Vertical axis shows the water depth (m). Unit is m^2s^{-1}.

Fig. 12 As in Fig. 7, but for the western equatorial Pacific (2˚S-2˚N, 160˚E-140˚W)

Fig. 13 As in Fig. 8, but for the annual mean for the western equatorial Pacific (2˚S-2˚N, 160˚E-140˚W)

Fig. 14 As in Fig. 10, but for the western equatorial Pacific (2˚S-2˚N, 160˚E-140˚W).

Fig. 15 The annual mean of the eddy kinetic energy averaged from the surface to 100m depth for (a) CTL and (b) DEP20_LEV05. Unit is Jm^{-3}. (c) Red and blue lines show the barotropic and baroclinic conversion terms for CTL, respectively. Unit is 10^{-5} kg/ms^3. (d) As in (c) but for the DEP20_LEV05.

Fig. 16 The annual cycle of the mean and eddy advection terms averaged over the region140˚W-90˚W, 2˚S-2˚N. Red and orange denote the mean and eddy advection terms for CTL. Blue and green denote the mean and eddy advection terms for DEP20_LEV05.

Table 1. List of experiments. "DEP" denotes the isotherm to be which SVS mixing is applied (˚C). "LEV" denotes the magnitude of the SVS mixing (m^2s^{-1}). Details are described in the right column. Background vertical diffusivity coefficients associated with SVS mixing are computed at every time step. The background vertical diffusivity coefficients in the equatorial Pacific and those outside of the region are linearly interpolated (c.f. Fig. 1).

Name of experiment	DEP	LEV	Details
CTL			An experiment without SVS mixing
DEP20_LEV025	20	0.25	
DEP20_LEV05	20	0.5	
DEP20_LEV1	20	1	
DEP15_LEV05	15	0.5	
DEP0_LEV05	0	0.5	
DEP15_LEVvar	15		Background vertical diffusivity coefficients are linearly decreased with depth from 1.0×10^{-4} m^2s^{-1} at the base of the mixed layer to 1.0×1.0^{-6} m^2s^{-1} at the 15˚C isotherm.

Table 2. The 20˚C isotherm depth (D_{20}) and thickness of thermocline (ΔD_{16-22}). The thickness of the thermocline is defined as the distance between isotherms of 16˚C and 22˚C. Unit is meter.

	D_{20}			ΔD_{16-22}		
	150˚E	180˚E	120˚W	150˚E	180˚E	120˚W
(a) CTL	165.1	157.4	59.1	50.0	45.6	75.2
(b) DEP20_LEV05	170.8	166.2	80.2	42.3	39.2	59.1
(c) DEP15_LEV05	176.3	172.5	80.3	59.5	66.1	120.1
(d) DEP0_LEV05	173.2	166.4	61.2	61.0	66.7	118.7
(e) DEP20_LEV025	168.0	163.1	70.8	45.3	41.0	64.3
(f) DEP20_LEV1	176.2	171.1	95.8	43.5	37.1	55.8
(g) DEP15_LEVvar	168.2	160.9	70.4	44.3	39.7	60.0

Table 3. Position of the core of the EUC, designated as the vertical grid point in which the annual mean of the zonal velocity averaged between 1˚S-1˚N has the maximum. Bold shows that the position of the core of the EUC of the run is deeper than that of CTL. Unit is meter.

	Position of the EUC core		
	150˚E	180˚E	120˚W
(a) CTL	158.9	158.9	85.2
(b) DEP20_LEV05	**181.9**	**181.9**	**95.4**
(c) DEP15_LEV05	**216.6**	**181.9**	**105.9**
(d) DEP0_LEV05	158.9	158.9	**95.4**
(e) DEP20_LEV025	**181.9**	158.9	85.2
(f) DEP20_LEV1	**181.9**	**181.9**	**105.9**
(g) DEP15_LEVvar	**181.9**	158.9	85.2

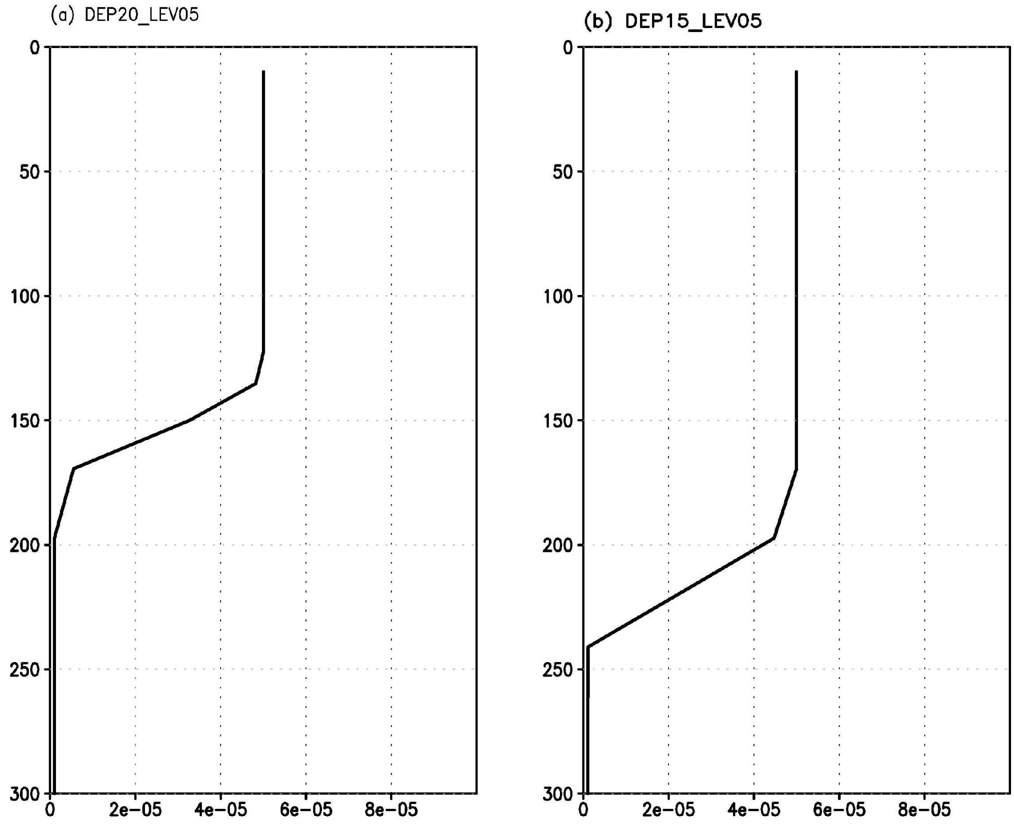

Fig. 1 Background vertical diffusivity coefficients at 0°N, 160°E for (a) DEP20_LEV05 and (b) DEP15_LEV05. Unit is m^2s^{-1}.

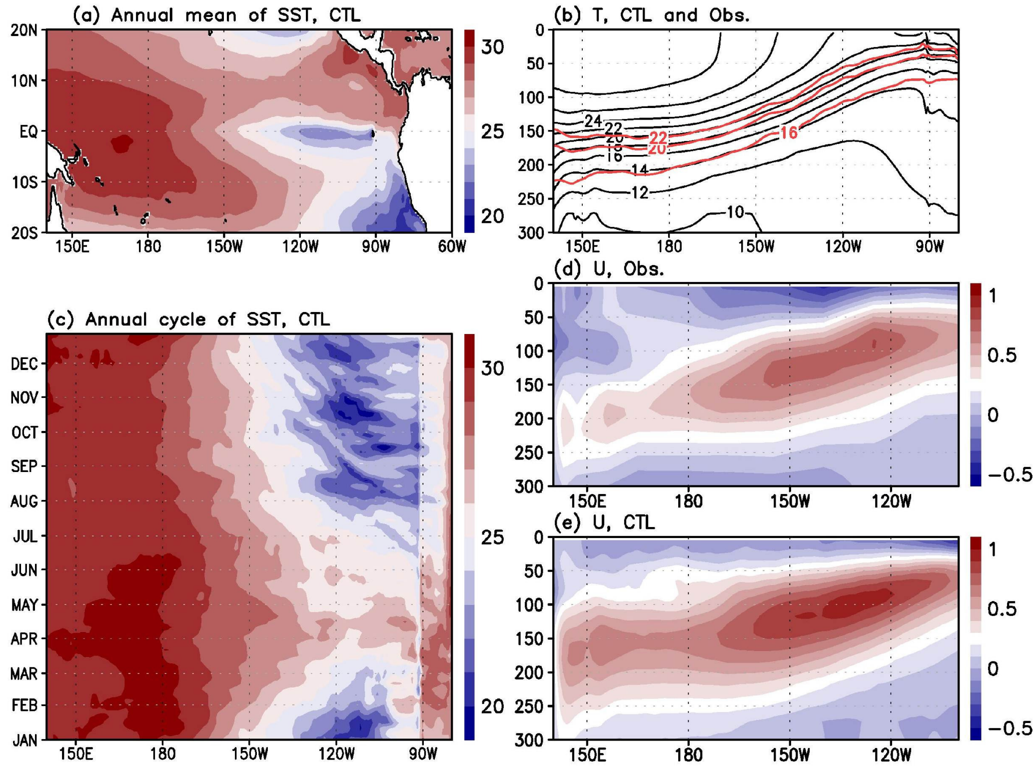

Fig. 2 (a) The annual mean of SST in CTL. (b) The annual mean of temperature averaged over the latitudinal band 2˚S-2˚N simulated by the OGCM (black) and observed (red). The 16, 20, and 22˚C isotherms are shown for the observed temperature. (c) The annual cycle of SST averaged over the latitudinal band 2˚S-2˚N. (d) Observed annual mean of zonal current averaged over the latitudinal band 1˚S-1˚N. (e) As in (d), but for the zonal current simulated in CTL. Unit is ˚C for (a-d) and ms^{-1} for (d and e).

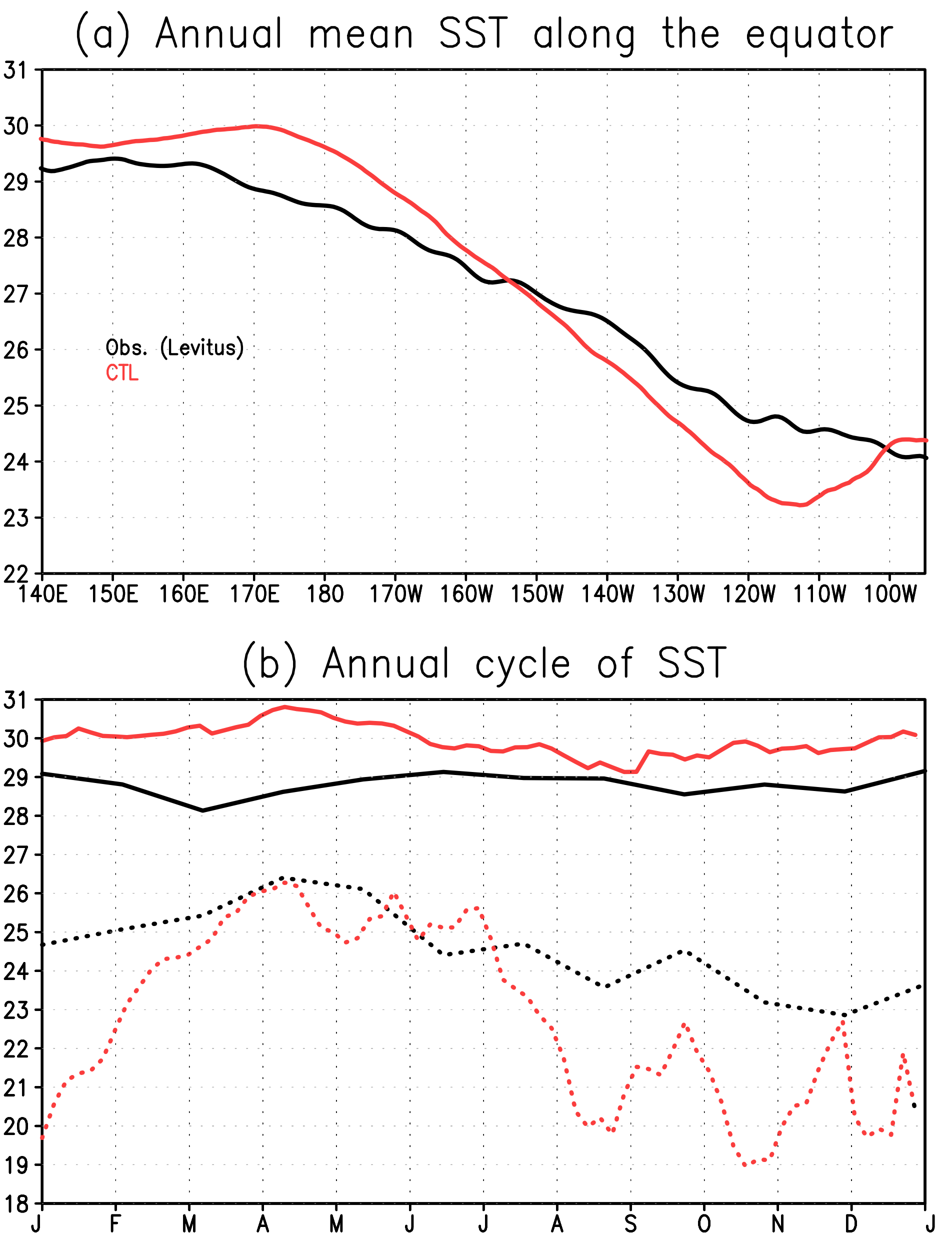

Fig. 3 (a) The annual mean of SST averaged over the latitudinal band 2˚S-2˚N. (b) The annual cycle of SST at 0˚N, 170˚E (solid) and 0˚N, 120˚W (dotted). Black and red shows the observation and model result, respectively. Unit is ˚C.

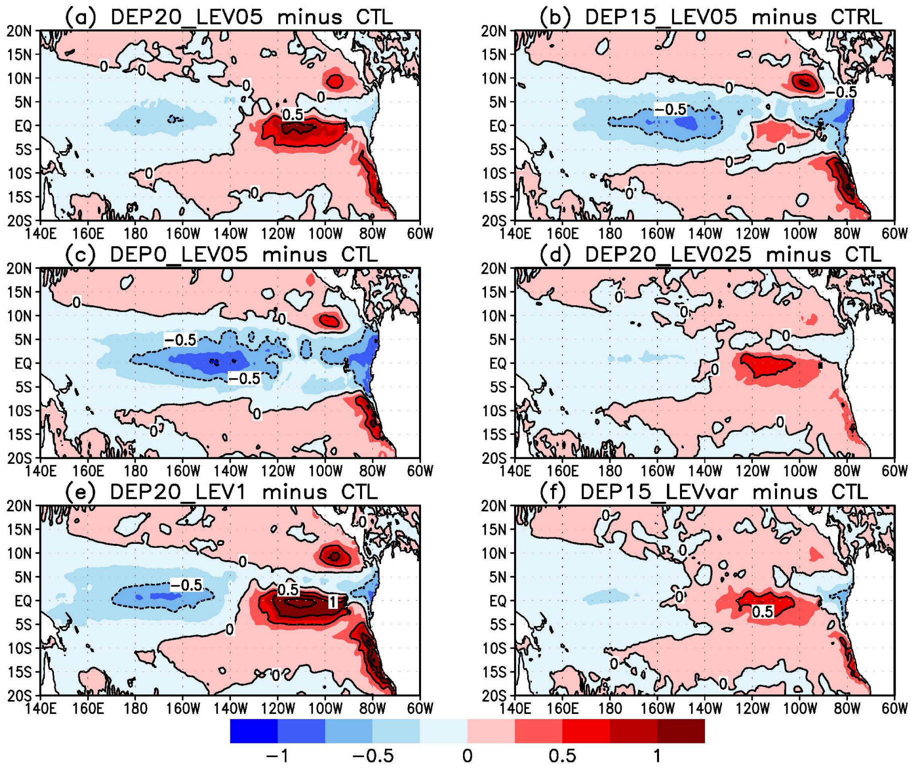

Fig. 4 A difference in the annual mean of SST between simulations with and without SVS mixing (with minus without SVS mixing). Unit is ˚C. The contour interval is 0.5˚C.

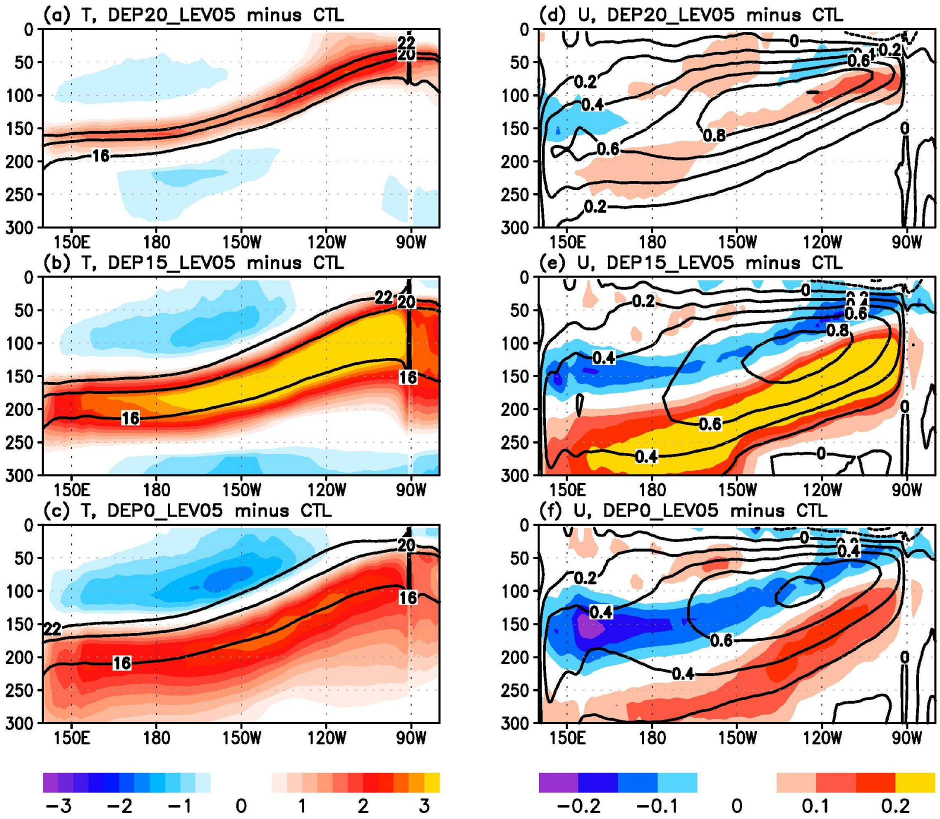

Fig. 5 (a-c) A difference in the annual mean of temperature along the equator between simulations with and without SVS mixing (with minus without SVS mixing). The contour shows the isotherm line of 16, 20, and 22˚C. Unit is ˚C. (d-f) The annual mean of zonal current along the equator (contour) and a difference in the annual mean of the zonal current between simulations with and without SVS mixing (color). Unit is ms^{-1}.

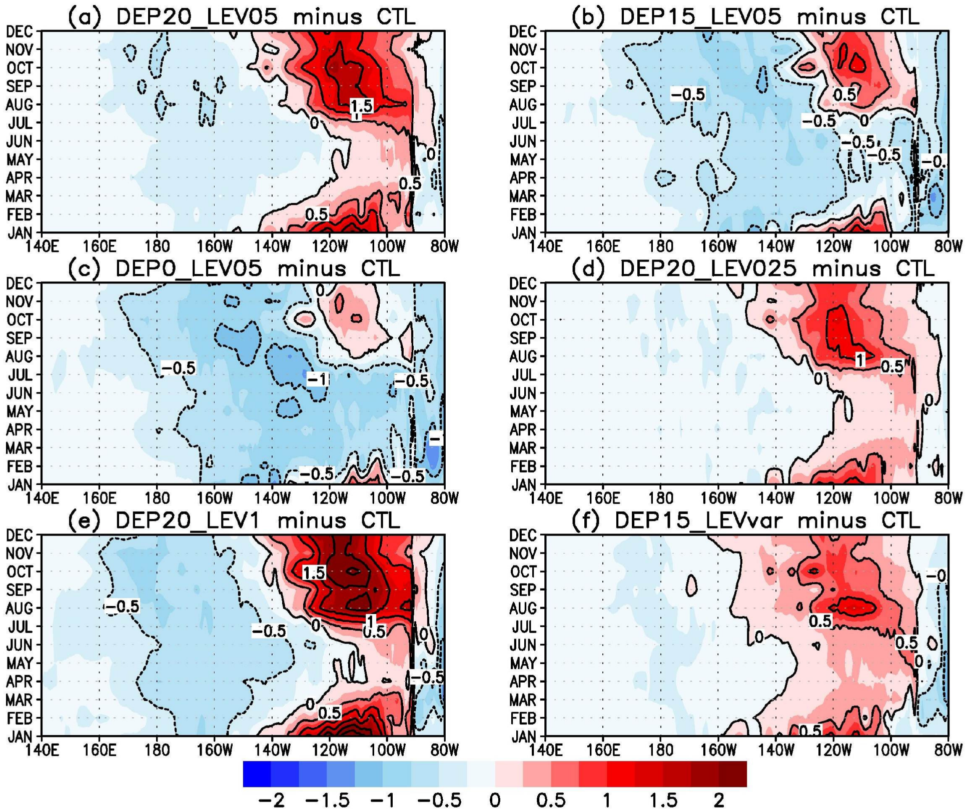

Fig. 6 As in Fig. 4, but for the annual cycle of SST averaged over the latitudinal band 2˚S-2˚N. The unit is ˚C.

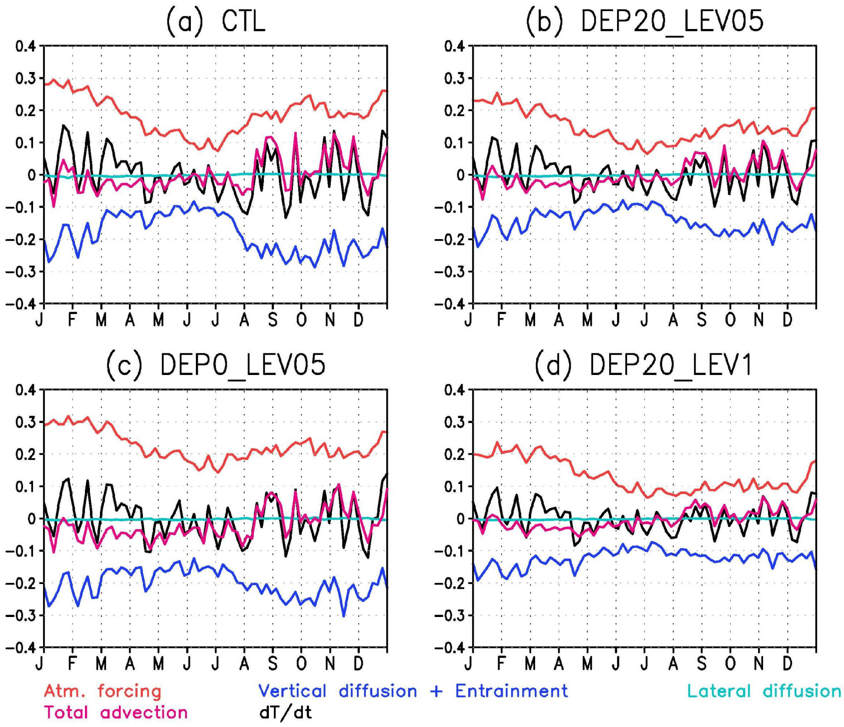

Fig. 7 The annual cycle of the tendency terms for the mixed layer heat budget averaged over the region 2˚S-2˚N, 140˚W-90˚W in (a) CTL, (b) DEP20_LEV05, (c) DEP0_LEV05, and (d) DEP20_LEV1. Red shows the atmospheric forcing term. Blue shows the sum of the entrainment and diffusive flux at the mixed layer base. Cyan and purple denote the lateral diffusion and advection, respectively. Black shows the temperature tendency. The unit is ˚C day^{-1}.

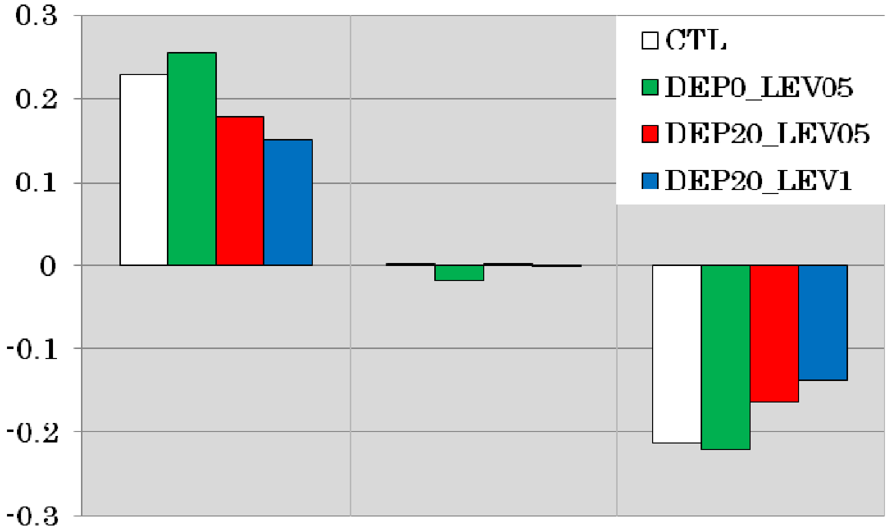

Fig. 8 The tendency terms for the mixed layer heat budget averaged over the region 2˚S-2˚N, 140˚W-90˚W for the July-February mean in CTL (white), DEP0_LEV05 (green), DEP20_LEV05 (red), and DEP20_LEV1 (blue). The left, central, and right part show the atmospheric forcing, advection, and vertical diffusion term, respectively. Unit is ˚C day^{-1}.

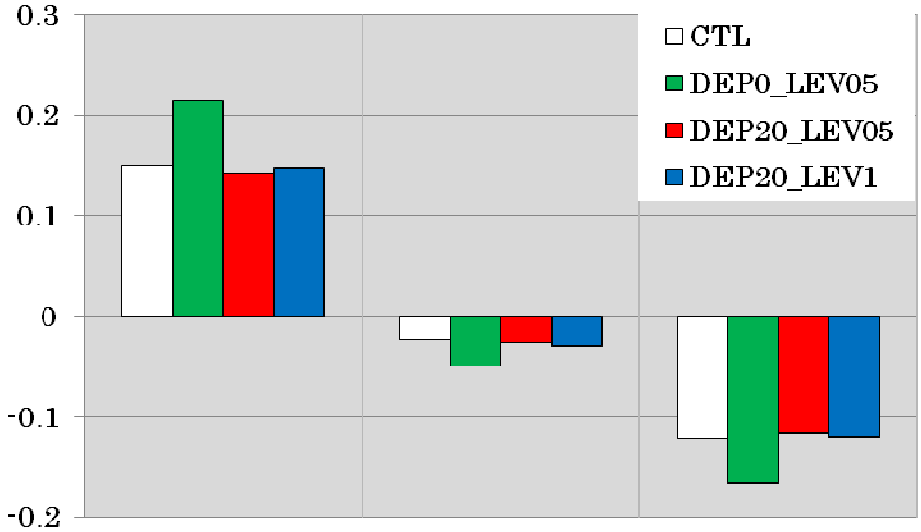

Fig. 9 As in Fig. 7, but for the March-June mean.

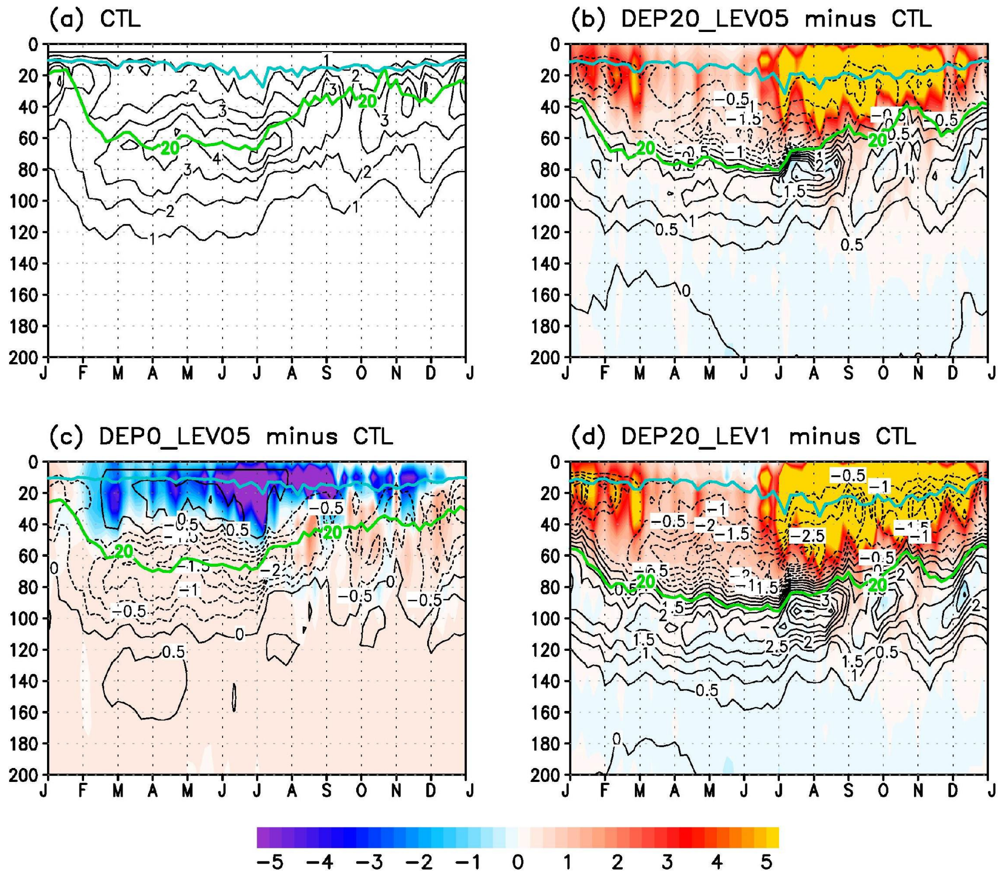

Fig. 10 (a) The annual cycle of the square of the buoyancy frequency (×10^{-4} s^{-2}, contour) averaged over the region 2˚S-2˚N, 120˚W-100˚W in CTL. (b-d) Difference in the vertical diffusivity coefficient (×10^{-4} m^{2}s^{-1}, color shaded) and the square of the buoyancy frequency (×10^{-4} s^{-2}, contour) between simulations with and without SVS mixing, respectively. Contours in cyan and green denote the annual cycle of the mixed layer depth and 20˚C isotherm, respectively.

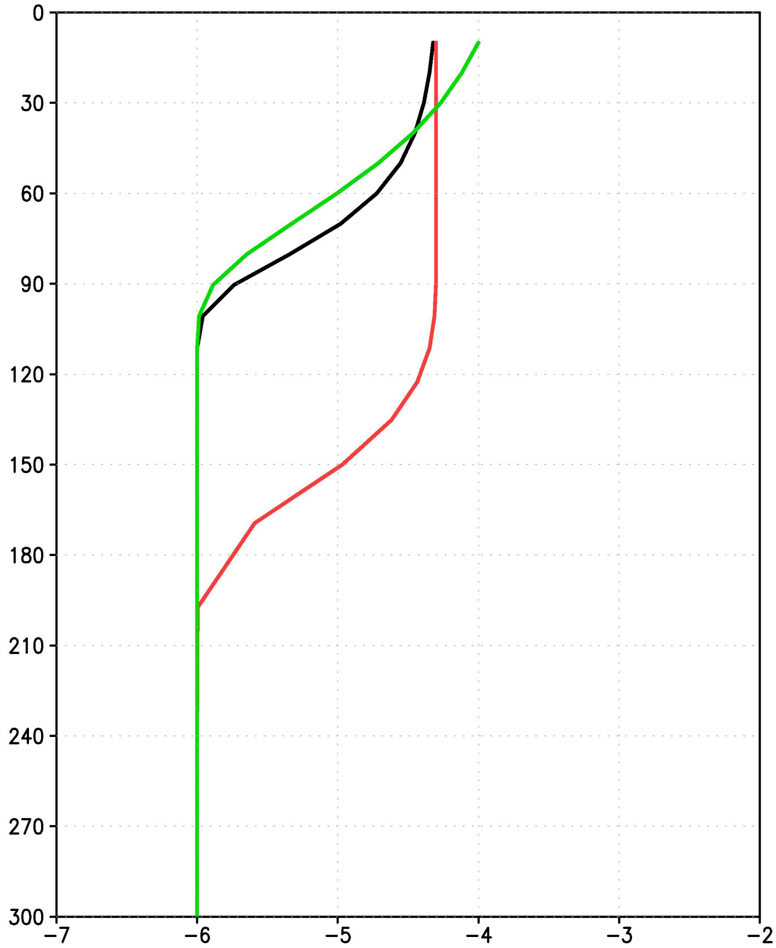

Fig. 11 (a) Vertical distribution of the annual mean of background vertical diffusivity coefficient averaged over the region 2˚S-2˚N, 120˚W-100˚W for DEP20_LEV05 (black), DEP15_LEV05 (red), and DEP15_LEVvar (green). The decimal logarithm is taken for the background vertical diffusivity coefficient. Vertical axis shows the water depth (m). Unit is m^2s^{-1}.

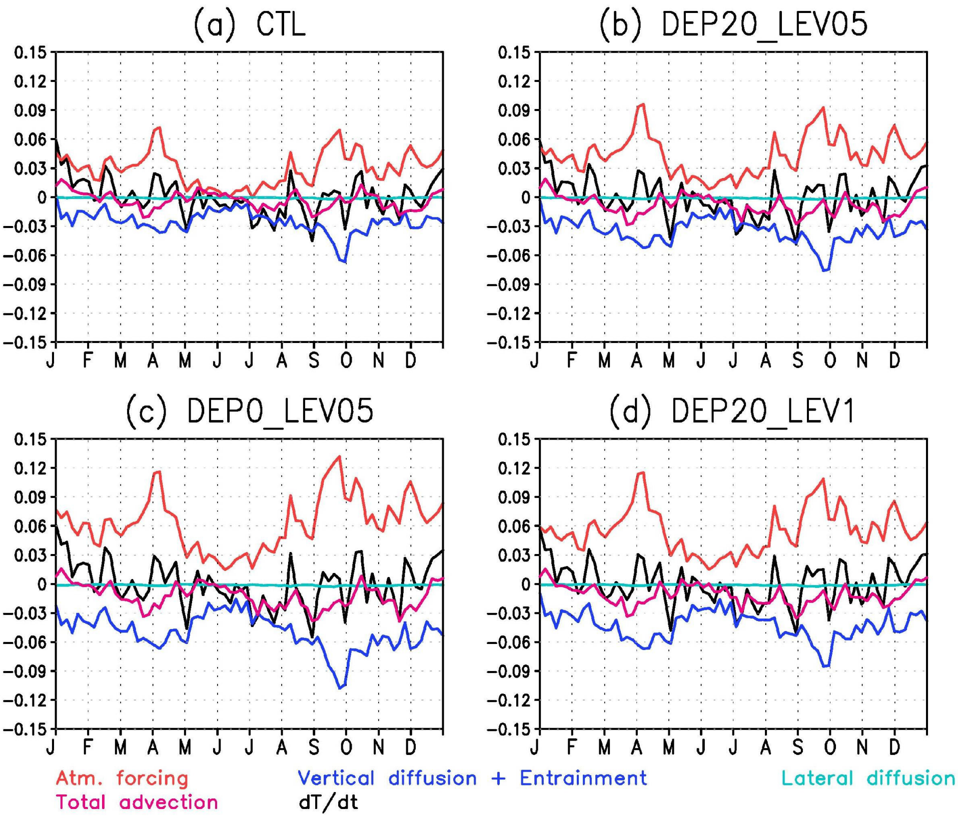

Fig. 12 As in Fig. 7, but for the western equatorial Pacific (2˚S-2˚N, 160˚E-140˚W).

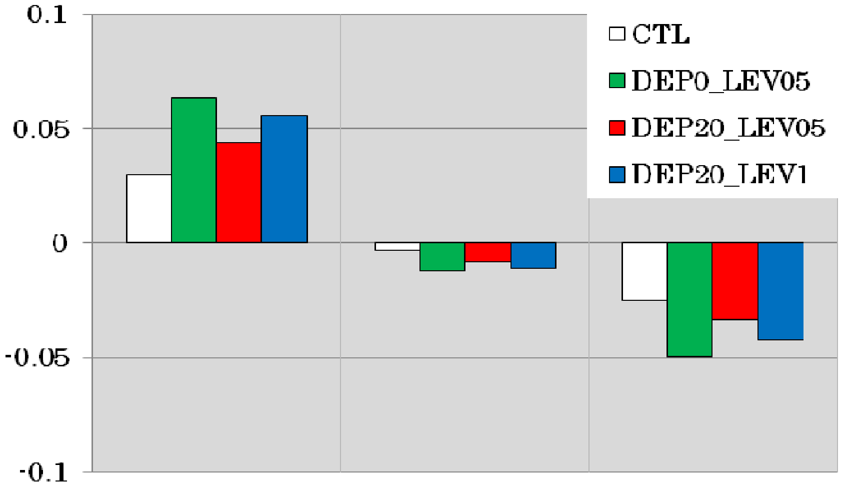

Fig. 13 As in Fig. 8, but for the annual mean for the western equatorial Pacific.

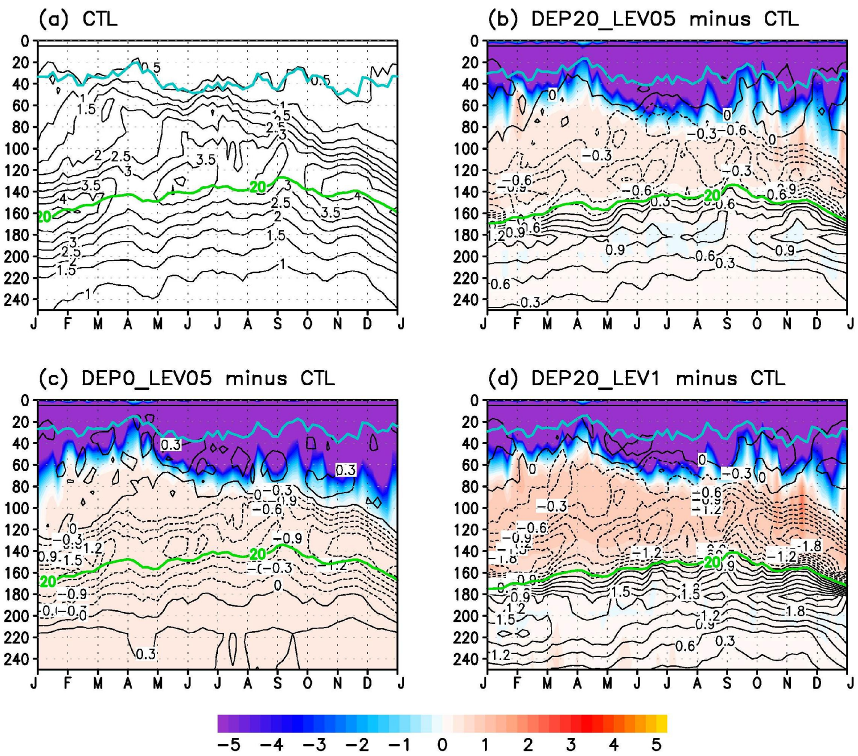

Fig. 14 As in Fig. 10, but for the western equatorial Pacific (2˚S-2˚N, 160˚E-140˚W).

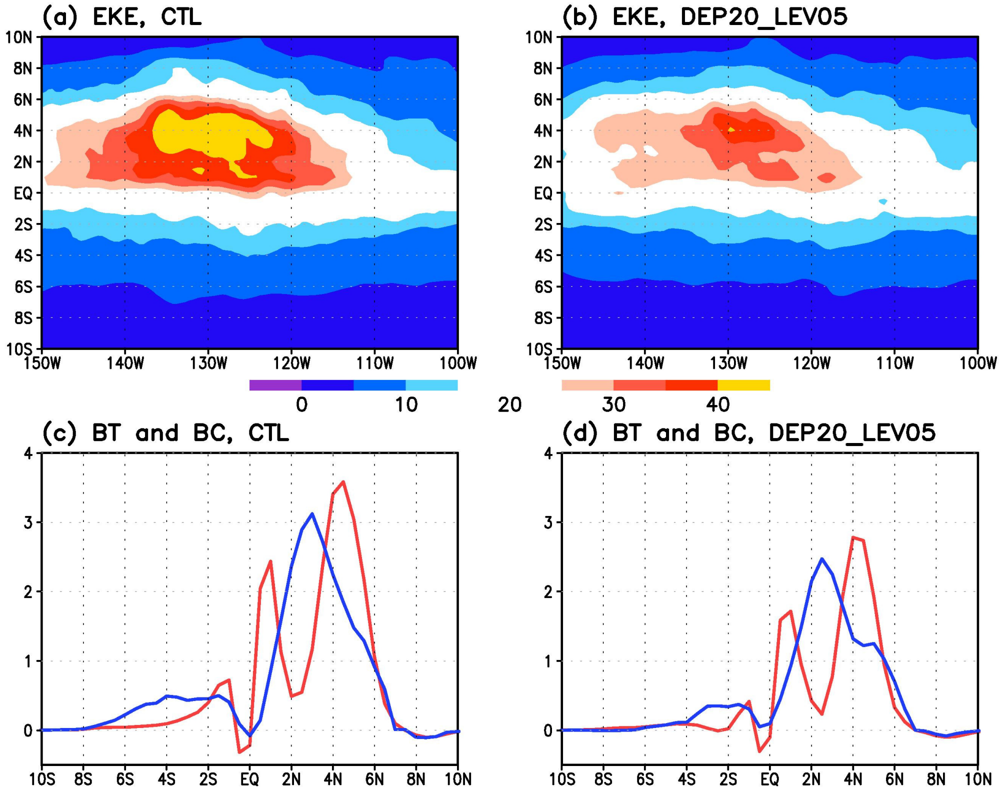

Fig. 15 The annual mean of the eddy kinetic energy averaged from the surface to 100m depth for (a) CTL and (b) DEP20_LEV05. Unit is Jm^{-3}. (c) Red and blue lines show the barotropic and baroclinic conversion terms for CTL, respectively. Unit is 10^{-5} kg/ms^3. (d) As in (c) but for the DEP20_LEV05.

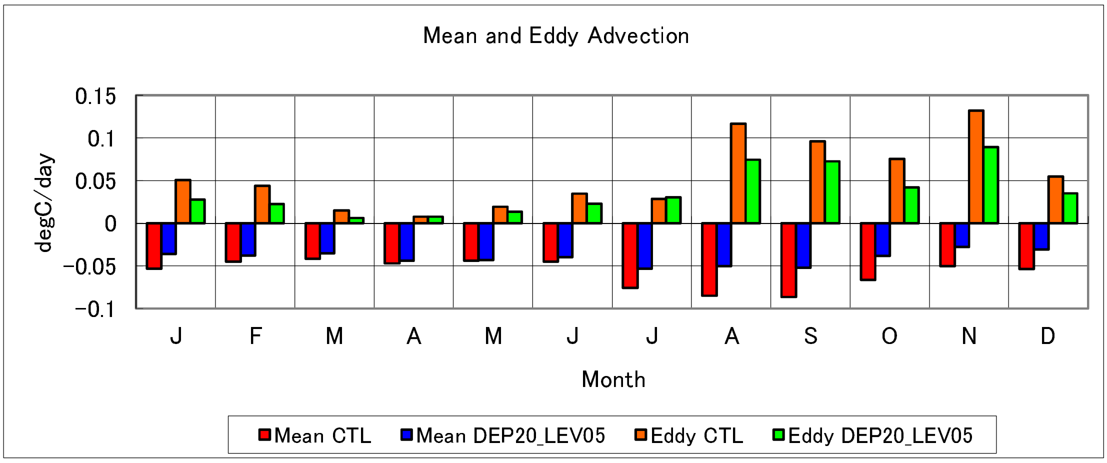

Fig. 16 The annual cycle of the mean and eddy advection terms averaged over the region140°W-90°W, 2°S-2°N. Red and orange denote the mean and eddy advection terms for CTL. Blue and green denote the mean and eddy advection terms for DEP20_LEV05.